


Article

Quantification and Analysis of Carrier-to-Interference Ratio in High-Throughput Satellite Systems

Zanyang Dong ^{1,2,*} , Longteng Yi ^{1,2}, Pengfei Qin ^{1,2}, Yejun Zhou ^{1,2}, Cheng Zhang ^{1,2} and Kang Liu ^{1,2}

¹ Institute of Telecommunication and Navigation Satellites, China Academy of Space Technology, Beijing 100094, China; ylongt@gmail.com (L.Y.); qinpf@zju.edu.cn (P.Q.); zhoyejuncast@foxmail.com (Y.Z.); orangezhang90@foxmail.com (C.Z.); liukang17@mails.ucas.ac.cn (K.L.)

² Innovation Center for Satellite Communication System, Beijing 100094, China

* Correspondence: zanydong@foxmail.com; Tel.: +86-187-1084-6102

Abstract: Recently, the demand for high data traffic transmission is experiencing unstoppable growth, and multi-beam high-throughput satellite (HTS) systems have proven to be effective solutions. However, how to manage and eliminate the co-channel interference caused by frequency reuse in multi-beam HTS systems is still a challenging issue. Motivated by this background, this paper begins with discussing the interference mechanism in the uplink and downlink of HTS systems and then uses the quantification method of carrier-to-interference ratio (CIR), whereby the influencing factors of the CIR are accordingly analyzed. In addition, the common CIR selection strategies are summarized and compared with each other in terms of their advantages and disadvantages. Based on the proposed CIR quantification and statistical selection methods, two frequency plan cases are simulated for the scenario of 19 beams with 4-color reuse. The results show that the proposed quantification and selection methods are rather practical and offer a feasible approach for frequency plan adjustment based on CIR optimization. Finally, a simulation analysis of the CIR under different power spectral density (PSD) values is conducted, and the results show that the PSD has a substantial impact on the CIR.

Keywords: multi-beam; high throughput satellite; frequency reuse; co-channel interference; carrier-to-interference ratio; frequency plan



Citation: Dong, Z.; Yi, L.; Qin, P.; Zhou, Y.; Zhang, C.; Liu, K. Quantification and Analysis of Carrier-to-Interference Ratio in High-Throughput Satellite Systems. *Electronics* **2023**, *12*, 3443. <https://doi.org/10.3390/electronics12163443>

Academic Editors: Qinghe Du, Li Sun, Hamed Ahmadi and Xiao Tang

Received: 18 July 2023

Revised: 28 July 2023

Accepted: 31 July 2023

Published: 15 August 2023



Copyright: © 2023 by the authors. Licensee MDPI, Basel, Switzerland. This article is an open access article distributed under the terms and conditions of the Creative Commons Attribution (CC BY) license (<https://creativecommons.org/licenses/by/4.0/>).

1. Introduction

Satellite communication services are available to any user within the service area of the satellite communication system, regardless of the user's location. This unique feature makes satellite communication systems attractive, especially in remote areas where ground network deployment is difficult or even impossible. In addition, satellite communication can provide various services such as television, broadcasting, telephone, and Internet services, making it indispensable to our hyperconnected society.

At present, multimedia application demand and data exchange are experiencing explosive growth [1], and multi-beam high throughput satellite (HTS) systems have proven to be one of the most promising solutions [2]. The antenna gain of multi-beam HTS systems is significantly higher when compared to the ones which use a single large beam to cover the entire service area. Since the first HTS was launched, the number of HTSs in geosynchronous orbit has increased year by year. The first generation of HTSs, represented by IPSTAR and AMC-15/16 satellites, employed spot beams with system throughput ranging from 2 to 5 Gbps. The second generation began to utilize narrow spot beam and frequency reuse technology with throughput ranging from 5 to 10 Gbps, represented by WildBlue-1 (35 spot beams) and Spaceway-3 (24 downlink beams) satellites. The third generation largely used narrow spot beams and frequency reuse technology, with a throughput of up to about 100 Gbps, represented by KA-SAT (82 spot beams) and ViaSat-1 (72 spot beams)

satellites. The fourth generation, most of which are currently under research, use large mesh deployable antennas that are capable of forming hundreds of narrower spot beams through beamforming technology, leading to a throughput of more than 300 Gbps, even up to 1 Tbps. ViaSat-2 (more than 100 spot beams), ViaSat-3, and SES17 (about 200 spot beams) are representative satellites. It can be seen that the development of HTS has led to a significant increase in system capacity, accompanied by substantial growth in the number of beams. Currently, mainstream satellite manufacturers in Europe and the United States have nearly 100 high-throughput satellites in orbit, and major satellite operators around the world are actively promoting the deployment of HTS satellites, with more than 1000 orders for HTS satellites around the world [3].

Figure 1 shows the difference between multi-beam and single-beam coverage. Since HTS multibeam antennas are spatially separated in space, enabling the same frequencies to be reused, multibeam coverage is an efficient way to exploit the system bandwidth, which is a very valuable yet expensive resource in any communication system. On the one hand, the frequency reuse technology greatly improves the total bandwidth of the system and then increases the system's capacity. Nevertheless, on the other hand, the side-lobe effect of multi-beam antennas will inevitably lead to co-channel interference between beams using the same frequency band [4,5], which occupies a more dominant position in the whole system interference compared with cross-polarization interference, adjacent channel interference, and other interferences. In reference [6], the authors claim that spot beam isolation and beam-to-beam interference become increasingly important as the number of beams is increased to tessellate a given geographic area, and they have to be carefully attended to. However, this paper does not focus on the quantification of the carrier-to-interference ratio (CIR). Therefore, it is necessary to research a method for quantifying the CIR (mainly co-channel interference) in multi-beam HTS systems, and based on this, the system capacity-oriented frequency allocation method is explored with a focus on the system's CIR optimization.

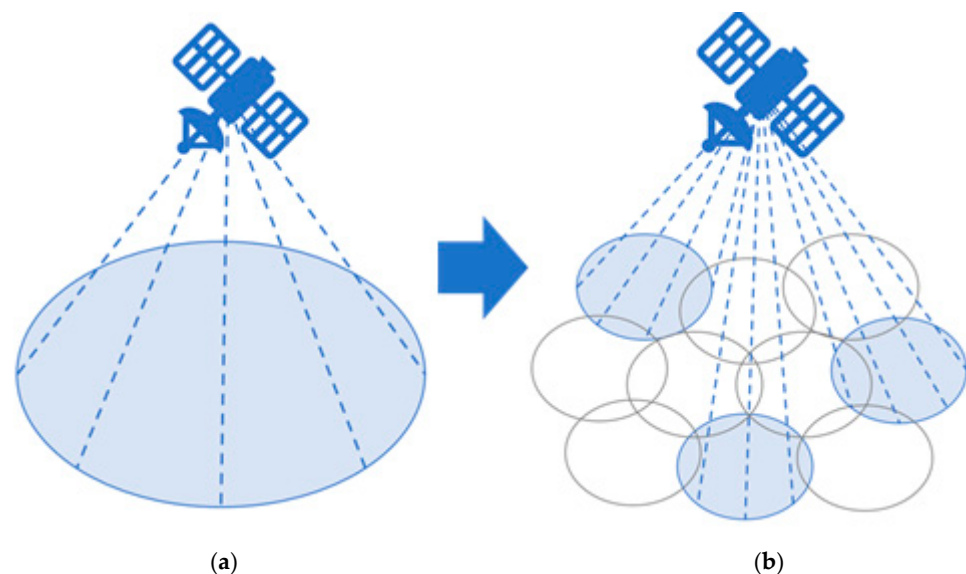


Figure 1. Different coverage modes in satellite systems: (a) single-beam coverage and (b) multi-beam coverage.

References [7–11] mention the role of the CIR in the link budget and give typical values of the CIR to explain or simulate relevant problems in satellite systems, but the typical values given by them are not uniform. For example, it is mentioned in reference [7] that when the frequency reuse factor is 1, 2, 3, or 4, the CIR is about 0 dB, 8 dB, 25 dB, or 30 dB, respectively. In particular, the range is between 14 dB and 34 dB when the frequency reuse factor is 4. In references [8,9], the CIR was set to 18 dB and 15 dB, respectively. In reference [10], the value of co-frequency co-polarization interference was set to 20 dB, while

the value of co-frequency cross-polarization interference and co-polarization interference of different frequencies were both set to 25 dB. In reference [11], the CIR was set to 16 dB for the reuse factor of 4. It is worth noting that these typical values are difficult to fully fit various real-world scenarios and are not persuasive due to a lack of theoretical support.

In addition, some researchers take the actual measured values of the CIR as the input to conduct their research. For example, in reference [12], the authors obtained the CIR geographical maps in dB for the KaSat coverage and came to the conclusion that the CIR increases when the beamwidth is narrower. This method may facilitate the accuracy of the research, but it is hard to obtain the data and inconvenient for theoretical research and model demonstration.

Furthermore, there are considerable efforts in the literature [13,14] devoted to developing the interference model and frequency reuse solutions in HTS, and a relatively concise calculation method was proposed for the calculation of the CIR. That is, the equivalent isotropically radiated power (EIRP) or on-board antenna gain value of the useful signal relative to the target user divided by the sum of the EIRP or on-board antenna gain value of interference signals relative to the target user. The calculation of the CIR is closer to the definition but is not conducive to the actual calculation, and the uplink and downlink are also not fully discussed. Similar to references [13,14], reference [15] provides an expression of co-channel interference power, which equals the sum of the power level of interference inside the target beam coming from all interfering beams of the target beam. However, this expression is conceptual and cannot indicate how we can derive the power level of interference. Reference [16] focused on the overall system design and introduced two software tools for system evaluation and analysis. In detail, the beam-drawing software developed by the University of Surrey can accomplish the gridding calculation of the CIR in the beam coverage area, and the calculation formula of the user link CIR is also known. However, the scenarios with multi-carriers in one beam related to the band plan and the influence of different frequency allocation schemes on the system CIR are not included in reference [16]. In summary, this has become a trend in CIR evaluation, from being computable to accurate and widely used. The difficulties lie in the in-depth analysis of the co-channel interference mechanism in multi-beam satellite systems and the derivation of closed-form expressions of the CIR that are compatible with various application scenarios. The application scenarios include not only geostationary orbit satellites but also non-geostationary orbit (NGSO) satellites, especially direct-to-satellite IoT (DtS-IoT) applications. In reference [17], the authors address massive MIMO in NGSO systems, which can substantially enhance spectral efficiency while bringing about inter-beam interference due to frequency reuse and the non-zero side lobes. In addition, the authors also emphasize the interference issue in waveform design, multiple access design, the co-existence of NGSO systems with other satellite systems and terrestrial networks, the emerging NGSO constellations, the inter-satellite links, and so on. Consequently, as the authors indicate, the interference quantification/management/cancellation should be paid more attention. In reference [18], the authors discuss the uplink transmission in the DtS-IoT whilst disregarding interference from other sources and focusing on the impact of terrestrial network interference on a satellite uplink transmission. As mentioned in this reference, it is quite possible to utilize shared frequency bands in areas where the terrestrial interference level is low enough. However, the terrestrial deployment over populated regions could drastically increase the uplink channel interference, which has to be addressed well. In reference [19], the authors focus on the random-access protocol based on Aloha for the MAC layer in DtS-IoT networks and introduce an intelligent traffic load distribution strategy with low implementation complexity, wherein the interference issue is addressed by applying successive interference cancellation (SIC) at the receiver for removing all copies once one of the messages is successfully decoded. The authors of [19] propose another traffic load distribution strategy based on successive convex approximation (SCA) in reference [20] and subsequently handle the interference between users in the same way. In reference [21], considering the intermittent link availability between the end devices and the gateways,

the authors propose a scheduling algorithm to ensure reliable communication and avoid packet drops/collisions. As discussed in [21], the communication between the end devices and the gateways is based on a spread spectrum modulation at the physical layer, and the importance of the interference issue lies in affecting the selection of the spreading factor, which suffers from a trade-off between the resulting bit rate, the transmission range, and the energy required to transmit. In reference [22], the authors focused on designing sparse constellations for the DTS-IoT with as few in-orbit DTS-IoT satellites as possible while guaranteeing the services. As mentioned, users' access to the radio channel is scheduled with a trade-off between mitigating interference and signaling traffic, which is consistent with the above references.

It is worth noting that more and more studies are being carried out to deal with co-channel interference. For example, satellite communication coding optimization design based on large frequency multiplexing factor and precoding technology can obviously eliminate the co-channel interference [23], which is especially suitable for full frequency multiplexing in the future. In addition, new communication schemes, such as the coded-beam high-throughput satellite system [24], are being investigated to avoid spectrum reuses and co-channel interference. However, the quantification of the CIR in current high-throughput satellite systems is still of great significance.

Aimed at the problem of dominant co-channel interference in multi-beam systems, this paper proposes a quantification method of the CIR for user uplink and downlink in multi-beam HTS systems, and the closed-form expressions are given. Furthermore, the influencing factors and selection strategies of the CIR are expounded. Finally, the feasibility of the proposed quantification method is verified through simulation.

The contribution of this paper is two-fold: first, a quantification method of the CIR for user uplink and downlink in multi-beam HTS systems is proposed; second, through numerical simulation, the effects of the frequency plan and PSD on the CIR are presented.

The remainder of the paper is organized as follows: Section 2 shows the model of the multi-beam HTS systems. In Section 3, a quantification method for the CIR is proposed with closed-form expressions. The influencing factors and selection strategies of the CIR are expounded in Section 4. In Sections 5 and 6, the simulation results and discussion are presented. Finally, Section 7 concludes the paper.

2. System Model

The HTS communication system consists of a space segment that includes the satellite constellation, a ground segment including gateway (GW) stations and large ground facilities for control, network operations, and backhauling, and a user segment with the user terminals deployed on fixed and mobile platforms (e.g., airplanes and ships) [25], as shown in Figure 2.

The space segment adopts the bent-pipe repeater, and the repeater is divided into the forward link and the return link. The forward link is from the ground gateway to the satellite and then to the ground users. The return link is just the opposite. According to the targeted object, the repeater can also be divided into the user link and the feeder link. The user link refers to the link between the satellite and the ground users, which can be further divided into the user uplink and user downlink. The feeder link refers to the link between the satellite and the ground gateway, which can be further divided into the feeder uplink and feeder downlink. The system utilizes the Ka band or the Q/V band as the communication frequency of feeder links and the Ka or Ku band for user links.

The common model for frequency reuse in high-throughput satellite systems is as follows [26]. The allocated bandwidth to a satellite, B_w , is first sliced into sub-bands, typically two or three. A guard band is necessary between the adjacent sub-bands. Then, right-hand or both right- and left-hand polarization are used with the sub-bands. Each sub-band and polarization type constitutes a color (see Figure 3). Then, each color is assigned to a spot beam, and Figure 4 shows the four-color reuse scheme among all the beams. Furthermore, as long as the colors do not overlap, they can be reused in separate

spot beams as many times as needed/possible (subject to various constraints including the antenna size, power limitation, pointing accuracy, and the system CIR discussed in this paper).

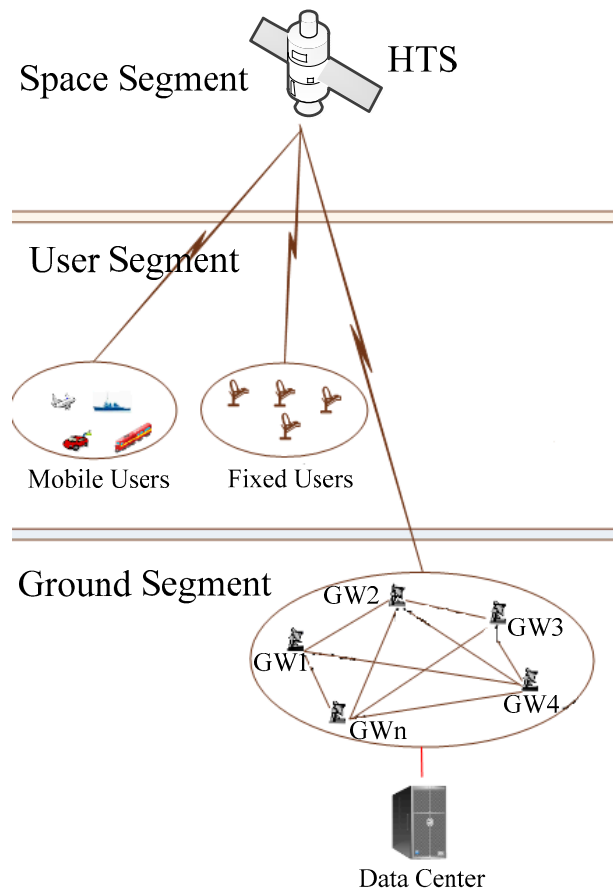


Figure 2. Architecture diagram of high-throughput satellite systems.

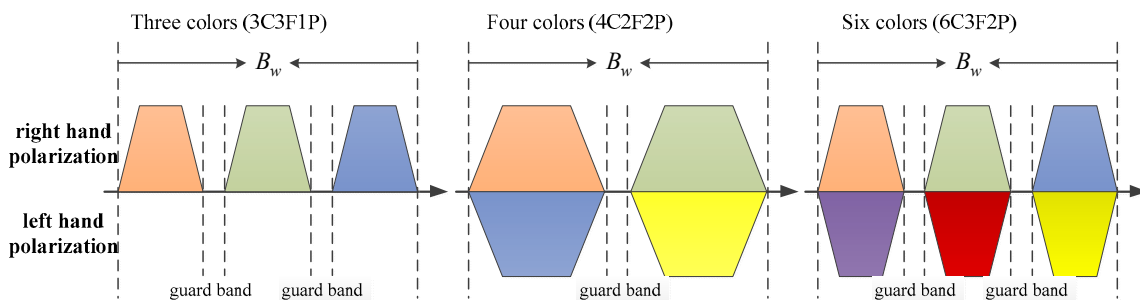


Figure 3. Examples of 3, 4, and 6 colors for frequency reuse.

Based on the frequency reuse scheme, the total bandwidth in the system can be calculated as follows:

$$B_{total} = \left(\frac{N_p N_b}{N_c}\right) B_w (1 - \eta_{guard}), \tag{1}$$

where N_p is the number of polarization (1 or 2), N_c is the number of colors, N_b is the number of beams, and η_{guard} is the guard band relative to the bandwidth of a single channel (typically 5% to 10%). For example, a 2.5 GHz allocated bandwidth can translate into 112.5 GHz total bandwidth for the satellite when allocated to 4 colors with 2 polarizations and 100 spot beams ($\eta_{guard} = 0.1$ for a 10% guard scheme).

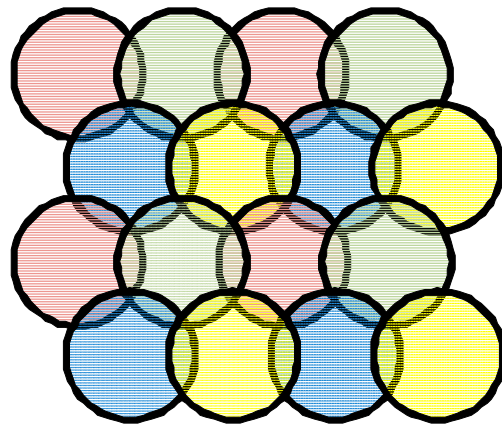


Figure 4. Four-color reuse scheme among all of the beams.

The common model for the link budget in such systems is as follows.
The propagation distance in free space can be obtained by:

$$d = \sqrt{R^2 + (R + H)^2 - 2R(R + H) \cos(\theta_1 - \theta_2) \cos(\varphi_1 - \varphi_2)}, \quad (2)$$

where d is the propagation distance in free space specified in meters; R is the earth radius specified in meters; H is the minimum distance between the satellite and the Earth's surface and the unit is also in meters; θ_1 and θ_2 are the longitudes of the satellite and the Earth station, respectively, in degrees; and φ_1 , φ_2 are the latitudes of the satellite and the Earth station, respectively, in degrees.

The propagation loss can be calculated by:

$$L = 10 \lg \left(\frac{4\pi d}{\lambda} \right)^2, \quad (3)$$

where L is the propagation loss in free space specified in decibels and λ is the working wavelength specified in meters.

The effective isotropic radiated power of transmitting antennas can be calculated by:

$$EIRP = P - L_t + G_t, \quad (4)$$

where $EIRP$ is the effective isotropic radiated power specified in dBW, P is the transmitting power specified in dBW, L_t is the feeder loss at the transmitter and the unit is in decibels, and G_t is the gain of the transmitting antenna specified in dBi.

The receiver's figure of merit can be obtained by:

$$G/T = G_r - 10 \lg \left(T_A + (10^{L_r/10} - 1) T_p + 10^{L_r/10} T_r \right), \quad (5)$$

where G/T is the receiver's figure of merit specified in dB/K, G_r is the gain of the receiving antenna specified in dBi, T_A is the output noise temperature of the antenna specified in K, L_r is the feeder loss at the receiver and the unit is in decibels, T_p is the feeder temperature specified in K, and T_r is the effective input noise temperature of the receiver specified in K.

The carrier-to-noise ratio (CNR) of the uplink and downlink can be then obtained, respectively:

$$[C/N]_u = [EIRP]_e - L_u - \Delta L_u + [G/T]_s - 10 \lg(kB), \quad (6)$$

$$[C/N]_d = [EIRP]_s - L_d - \Delta L_d + [G/T]_e - 10 \lg(kB), \quad (7)$$

where $[C/N]_u$ and $[C/N]_d$ are the CNRs of the uplink and downlink, respectively, specified in decibels; $[EIRP]_e$ and $[EIRP]_s$ are the effective isotropic radiated power of the earth

station (or the terminal) and the satellite, respectively, specified in dBW; L_u and L_d are the propagation losses in the free space of the uplink and downlink, respectively, specified in decibels; ΔL_u and ΔL_d are the additional losses (including atmospheric absorption, pointing error, and polarization loss) of the uplink and downlink, respectively, specified in decibels; $[G/T]_s$ and $[G/T]_e$ are the figures of merit of the satellite and the Earth station (or the terminal), respectively, specified in dB/K; k is the Boltzmann's constant; and B is the receiver's bandwidth specified in Hz.

Based on the CNR of the uplink and downlink, $[C/N]_u$ and $[C/N]_d$, the total CNR of the entire link, C/N , for a conventional frequency translation satellite, can be approached as follows [13]. $[C/N]_u$, $[C/N]_d$, and C/N are all specified in decibels.

$$C/N = 10\lg\left(\frac{1}{1/10^{[C/N]_u/10} + 1/10^{[C/N]_d/10}}\right). \quad (8)$$

By combining the total CNR, C/N , and the system CIR, C/I , which is just our research focus in this paper, we can obtain the carrier-to-interference-plus-noise ratio $C/(I+N)$ [13]:

$$C/(I+N) = 10\lg\left(\frac{1}{1/10^{(C/I)/10} + 1/10^{(C/N)/10}}\right), \quad (9)$$

followed by the ratio of the signal power per bit to noise power spectrum E_b/N_0 :

$$E_b/N_0 = C/(I+N) - 10\lg R_b + 10\lg(B), \quad (10)$$

where R_b is the information transmission rate specified in bps.

Based on E_b/N_0 , we can derive the available highest-level modulation coding mode and then the system capacity. Through the whole derivation process, we can conclude the importance of C/I for the system capacity budget.

3. Quantification Method of CIR

The system CIR refers to the power ratio of the carrier signal to the sum of interference signals. As for the calculation of the satellite system CIR, the CIRs of the forward uplink (i.e., feeder uplink), forward downlink (i.e., user downlink), return uplink (i.e., user uplink), and return downlink (i.e., feeder downlink) should be comprehensively considered. The details are as follows:

$$(C/I)_f = 10\lg\left(\frac{1}{1/10^{(C/I)_{fu}/10} + 1/10^{(C/I)_{fd}/10}}\right), \quad (11)$$

$$(C/I)_b = 10\lg\left(\frac{1}{1/10^{(C/I)_{bu}/10} + 1/10^{(C/I)_{bd}/10}}\right), \quad (12)$$

where C is the carrier power and I is the interference signal power, $(C/I)_{fu}$, $(C/I)_{fd}$, $(C/I)_{bu}$, $(C/I)_{bd}$, $(C/I)_f$, and $(C/I)_b$ refer to the CIR of the forward uplink, forward downlink, return uplink, return downlink, the entire forward link, and return link, respectively.

In this paper, the uplink interference and downlink interference are discussed. The quantification method of user's uplink interference and downlink interference (corresponding to return uplink and forward downlink) is expounded. Due to the same principle, feeder uplink interference and feeder downlink interference (corresponding to the forward uplink and return downlink) can be quantified in a similar way. Moreover, the number and location of the ground gateways are deterministic, making it easier to handle the feeder link. Based on the above results, the system CIR can be obtained according to Equations (11) and (12).

Next, we will discuss the quantification method of the CIR for user uplink and downlink.

3.1. User Uplink

The schematic diagram of co-channel interference in the user uplink is shown in Figure 5. The green continuous line represents the uplink of the useful signal, intended as the one from the actual user location to the satellite. The green dotted line represents the connection between the center of the cell that targets the user and the satellite. The red continuous line represents the uplink of the i -th interference signal; the red dotted line represents the connection between the center of the cell, where the i -th interfering user is located, and the satellite; P_1 represents the terminal transmitting power of the target user; $G_{T,1}$ represents the terminal antenna transmitting gain of the target user; L_1 represents the path loss of the uplink of the useful signal; θ_1 represents the deviation angle of the uplink of the useful signal from its own cell center; $G_1(\theta)$ represents the on-board antenna receiving gain function for the uplink of the useful signal; P_i represents the terminal transmitting power of the i -th interfering user; $G_{T,i}$ represents the terminal antenna transmitting gain of the i -th interfering user; L_i represents the path loss of the uplink of the i -th interfering user; θ_i represents the deviation angle of the uplink of the i -th interfering signal from its own cell center; $G_i(\theta)$ represents the on-board antenna receiving gain function for the uplink of the i -th interfering signal; and $\psi_{c1,i}$ represents the deviation angle of the uplink of the i -th interfering signal from the center of the cell that targets the user.

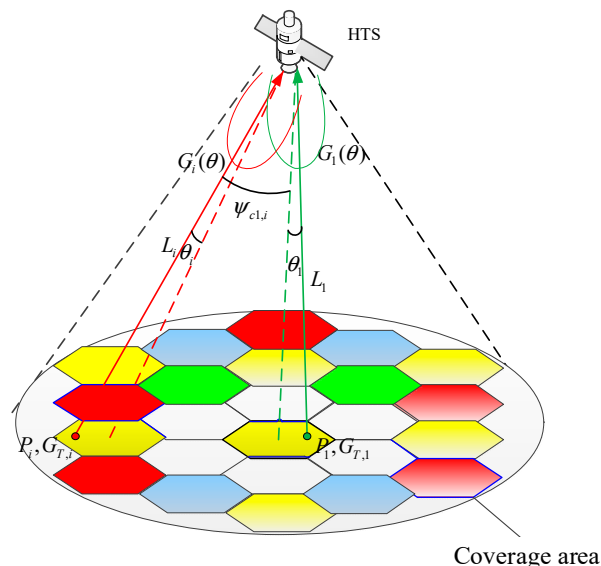


Figure 5. Schematic diagram of co-channel interference in the user uplink.

The CIR of the uplink for the target user is (without special instructions, the interference in the following section refers to the co-channel interference):

$$\begin{aligned}
 (C/I)_{bu} &= \frac{(C)_{bu}}{\sum_i (I_i)_{bu}} \\
 &= \frac{P_1 G_{T,1} G_1(\theta_1) / L_1}{\sum_i P_i G_{T,i} G_i(\psi_{c1,i}) / L_i}
 \end{aligned}
 \tag{13}$$

where $(I_i)_{bu}$ is the power of the i -th interference signal received on the satellite and $(C)_{bu}$ is the power of the useful signal received on the satellite.

Since uplink power control (UPC) is often adopted in HTS systems, the differences due to terminal transmitting power, terminal antenna gain, and path loss in different uplinks will be compensated. Finally, the signal powers received by the satellite from different terminals are uniform, namely:

$$P_i G_{T,i} G_i(\theta_i) / L_i = P_1 G_{T,1} G_1(\theta_1) / L_1.
 \tag{14}$$

Substituting Equation (14) into Equation (13), we can obtain:

$$\begin{aligned}
 (C/I)_{bu} &= \frac{P_1 G_{T,1} G_1(\theta_1) / L_1}{\sum_i P_i G_{T,i} G_1(\psi_{ci,i}) / L_i} \\
 &= \frac{P_1 G_{T,1} G_1(\theta_1) / L_1}{\sum_i G_1(\psi_{ci,i}) P_1 G_{T,1} G_1(\theta_1) / L_1 / G_i(\theta_i)} \\
 &= 1 / \sum_i \frac{G_1(\psi_{ci,i})}{G_i(\theta_i)}
 \end{aligned}
 \tag{15}$$

It can be seen that uplink interference occurs when the signal transmitted by the interfering user falls into the on-board receiving antenna for the target user. With the participation of the UPC, the CIR of the uplink is not related to the position of the target user but rather only to the positions of interfering users.

3.2. User Downlink

The schematic diagram of co-channel interference in the user downlink is shown in Figure 6. The green continuous line represents the downlink of the useful signal. The green dotted line represents the connection between the center of the cell, where the target user is located, and the satellite. The red continuous line represents the downlink of the i -th interference signal; the red dotted line represents the connection between the center of the cell, where the i -th interfering user is located, and the satellite; P_1 represents the on-board transmitting power to the target user; L_1 represents the path loss of the downlink of the useful signal; θ_1 represents the deviation angle of the downlink of the useful signal from its own cell center; $G_1(\theta)$ represents the on-board antenna transmitting gain function for the downlink of the useful signal; P_i represents the on-board transmitting power to the i -th interfering user; L_i represents the path loss of the downlink of the i -th interfering user; θ_i represents the deviation angle of the downlink of the i -th interfering signal from its own cell center; $G_i(\theta)$ represents the on-board antenna transmitting gain function for the downlink of the i -th interfering signal; and $\psi_{ci,1}$ represents the deviation angle of the downlink of the useful signal from the cell center of the i -th interfering user.

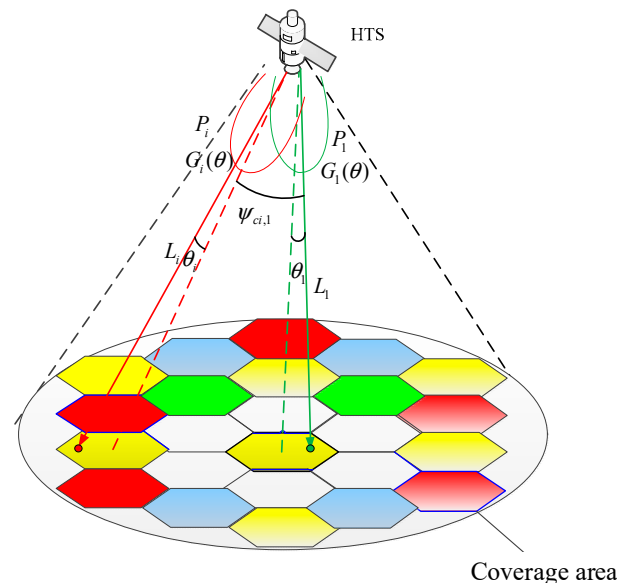


Figure 6. Schematic diagram of co-channel interference in the user downlink.

The CIR of the downlink for the target user is:

$$(C/I)_{fd} = \frac{(C)_{fd}}{\sum_i (I_i)_{fd}} = \frac{P_1 G_1(\theta_1) / L_1}{\sum_i P_i G_i(\psi_{ci,1}) / L_i} \tag{16}$$

where $(I_i)_{fd}$ is the power of the i -th interference signal received by the target user and $(C)_{fd}$ is the power of the useful signal received by the target user.

In the downlink, due to the same propagation path of the useful signal and interference signals, L_1 can be eliminated in Equation (16) and then we have:

$$(C/I)_{fd} = \frac{P_1 G_1(\theta_1)}{\sum_i P_i G_i(\psi_{ci,1})}. \quad (17)$$

It can be seen that the interference mechanism in the downlink is different from that in the uplink. The downlink interference at the user's receiver comes from beams pointed at other users. Thus, the interference occurs when these spurious signals fall into the receiving antenna of the target user. Therefore, the CIR of the downlink for the target user is not related to the positions of the interfering users but instead only to the position of the target user.

3.3. Multi-Carrier Scenarios

The above general quantification method of the CIR is based on the assumption that there is only one continuous frequency band in each beam. For very-high-throughput satellite (VHTS) communication systems, the frequency bands within each beam may not be continuous, and the two multiplexed beams do not belong to the absolute same color. The quantification method can be improved adaptively as follows.

Each sub-carrier is treated as a "beam". It is worth noting that the possible area where users are located for each sub-carrier within the same beam is the same, that is, the entire beam area. In order to help understand this conclusion better, we illustrate the equivalent representation of an interfering beam with multi-carriers in Figure 7.

In Figure 7, the green line, which points to a beam with a yellow color, represents the useful signal for the target user. The transmitting power and the frequency band of the useful signal are denoted as P_1 and $[f_1, f_2]$, respectively. The other beams with a yellow color are interferers naturally. As mentioned above, the interfering power is the sum of that coming from every interfering beam, i.e., $I = \sum_i I_i$. However, in multi-carrier scenarios, it should be emphasized that beams with the same color do not occupy the identical frequency band, although their frequency bands overlap to a certain degree. That is to say, part of the transmitting power of an interfering beam, although not all, will cause the interference in the beam where the target user is located. Taking the i -th interfering beam for example, as shown in Figure 7, we denote the transmitting power, the total bandwidth, and the number of carriers in this beam as P_i , B_i , and N_i , respectively. Specifically, the frequency band of the j -th carrier ($j \leq N_i$) is denoted as $[f_{ij}^{start}, f_{ij}^{stop}]$ in a generic way. It is easy to conclude that:

$$B_i = \sum_{j=1}^{N_i} (f_{ij}^{stop} - f_{ij}^{start}). \quad (18)$$

If there are no guard bands between the frequency bands of these carriers, then $B_i = f_{iN_i}^{stop} - f_{i1}^{start}$. It is worth noting that there is no difference in the spatial orientation among all the carriers. Each carrier can serve a user located at any position belonging to the beam area. Therefore, a carrier can be modelled as a virtual beam, and an interfering real beam with multi-carriers can be modelled as the addition of multiple virtual beams. As a result, the interference coming from the i -th interfering beam is equal to the sum of the contribution of all the virtual beams: $I_i = \sum_j I_{ij}$.

The transmitting power of the j -th virtual beam ($j \leq N_i$) is denoted as P_{ij} , and $P_i = \sum_j P_{ij}$. Furthermore, because the multi-carriers in a real beam shall share the same travelling wave tube amplifier (TWTA), the power spectral density (PSD) of them are equal,

i.e., the transmitting power of each carrier, or each virtual beam, is proportional to its own bandwidth. Hence, P_{ij} can be calculated by:

$$P_{ij} = \frac{(f_{ij}^{stop} - f_{ij}^{start}) P_i}{B_i}. \tag{19}$$

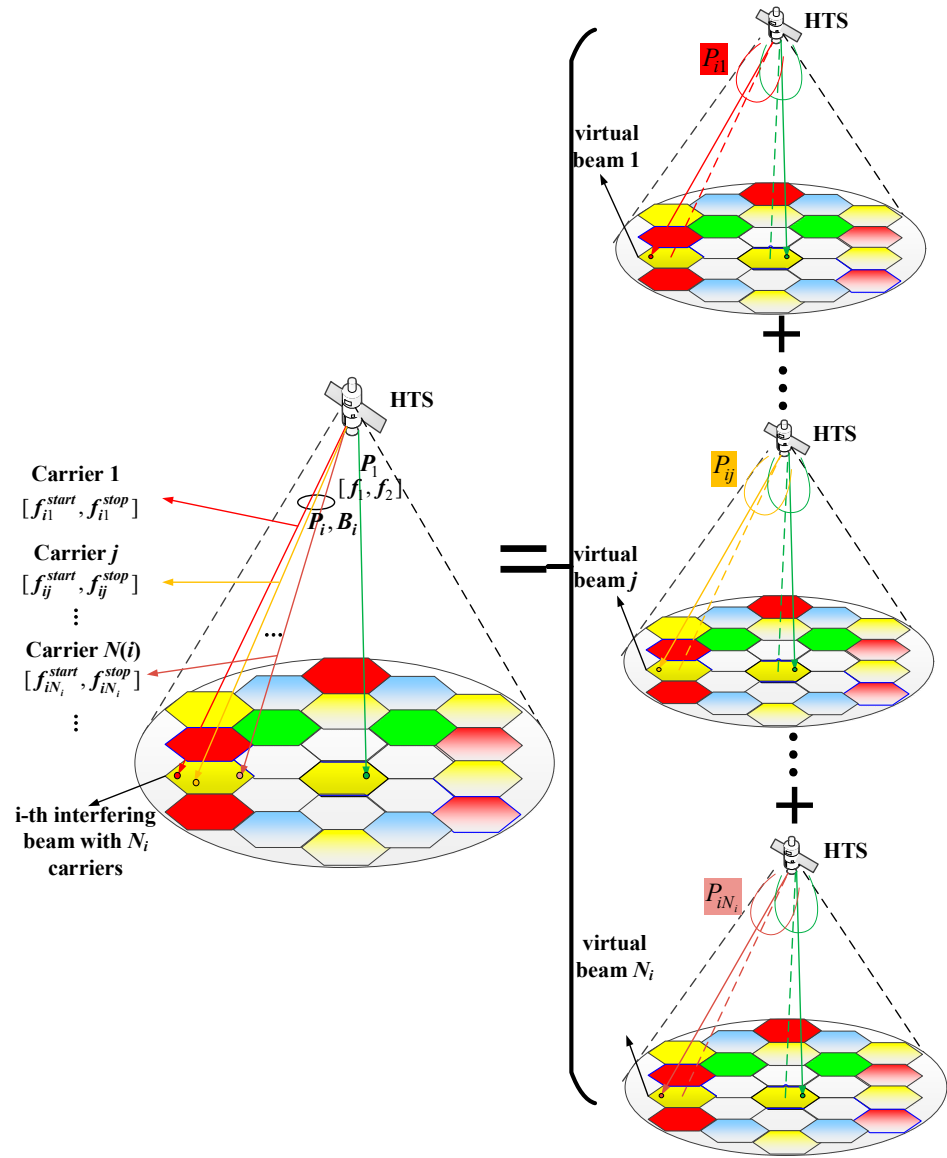


Figure 7. The equivalent representation of an interfering beam with multi-carriers.

Furthermore, a fraction of P_{ij} would create an interference in the target beam and the proportion depends on the overlapping of $[f_1, f_2]$ and $[f_{ij}^{start}, f_{ij}^{stop}]$. Thus, the weighted power, \tilde{P}_{ij} , would be:

$$\tilde{P}_{ij} = \frac{[(f_{ij}^{stop} - f_{ij}^{start} + f_2 - f_1) - (\max(f_{ij}^{stop}, f_2) - \min(f_{ij}^{start}, f_1))] P_{ij}}{f_{ij}^{stop} - f_{ij}^{start}}. \tag{20}$$

As described in Section 3.2, the interfering power coming from the j -th virtual beam would be:

$$I_{ij} = \tilde{P}_{ij} G_i(\theta). \tag{21}$$

To summarize, in multi-carrier scenarios, Equation (17) should turn into:

$$\begin{aligned}
 (C/I)_{fd} &= \frac{P_1 G_1(\theta_1)}{\sum_i I_i} = \frac{P_1 G_1(\theta_1)}{\sum_i \sum_{j=1}^{N_i} I_{ij}} = \frac{P_1 G_1(\theta_1)}{\sum_i \sum_{j=1}^{N_i} \tilde{P}_{ij} G_i(\theta)} \\
 &= \frac{P_1 G_1(\theta_1)}{\sum_i \sum_{j=1}^{N_i} \frac{[(f_{ij}^{stop} - f_{ij}^{start} + f_2 - f_1) - (\max(f_{ij}^{stop}, f_2) - \min(f_{ij}^{start}, f_1))] P_i G_i(\theta)}{f_{ij}^{stop} - f_{ij}^{start}}} \\
 &= \frac{P_1 G_1(\theta_1)}{\sum_i \sum_{j=1}^{N_i} \frac{[(f_{ij}^{stop} - f_{ij}^{start} + f_2 - f_1) - (\max(f_{ij}^{stop}, f_2) - \min(f_{ij}^{start}, f_1))] P_i G_i(\theta)}{B_i}}
 \end{aligned} \tag{22}$$

In the same way, if the target beam also includes multi-carriers, and the total transmitting power and bandwidth are denoted as P_0 and B_0 , respectively, Equation (22) should turn into:

$$(C/I)_{fd} = \frac{(f_2 - f_1) P_0 G_1(\theta_1) / B_0}{\sum_i \sum_{j=1}^{N_i} \frac{[(f_{ij}^{stop} - f_{ij}^{start} + f_2 - f_1) - (\max(f_{ij}^{stop}, f_2) - \min(f_{ij}^{start}, f_1))] P_i G_i(\theta)}{B_i}} \tag{23}$$

4. Influencing Factors and Selection Strategies of the CIR

4.1. Influencing Factors

According to the proposed quantification method, it can be summarized that the influencing factors of the CIR include but are not limited to the following aspects:

- (1) System coverage: such as the service area, beam number, overlapping level of these beam areas, etc.

It is evident that the system coverage can affect the distance between the interfering beams and the target beam, hence yielding a quite different CIR. We can easily judge that the one with a larger distance corresponds to better performance in the CIR.

- (2) Frequency plan.

The frequency plan can affect the number of interfering beams, the distance between the interfering beams and the target beam, and the overlapping frequency band between them. In Section 5, we can further conclude the significant effect of the frequency plan on the system CIR through simulation.

- (3) Antenna radiation pattern.

The antenna radiation pattern reflects different gain functions in Equations (15) and (17), thus having a significant effect on the system CIR. It is worth noting that the gain function can be obtained through numeric processing of the antenna radiation pattern. Figure 8 shows an example of the antenna radiation pattern.

- (4) User terminal locations.

The user terminal locations can affect the deviation angle in Equations (15) and (17). In detail, as mentioned before, the CIR of the uplink is not related to the position of the target user but rather only to the positions of interfering users. The CIR of the downlink for the target user is not related to the positions of the interfering users within their respective beams but rather only to the position of the target user.

- (5) Antenna imperfection, which influences the cross-polarization interference.
- (6) Nonlinearity of amplifiers, which generates nonlinear interference. For instance, spectrum regeneration causes interference among adjacent beams, etc.

4.2. Selection Strategies

The premise of quantifying the CIR mentioned above is that the locations of the target user and interfering users are known. However, in mobile application scenarios, the

location of any user is random and time varying. Therefore, the selection of CIR values is a practical challenge. The specific selection strategies are as follows:

- (1) **Select typical values:** This method is the most simple and feasible, but it cannot truly reflect the characteristics of the system. The link budget based on this method can only estimate the system capacity roughly rather than predict it accurately.
- (2) **Take values according to the antenna pattern and coverage requirements:** According to the actual pattern of each antenna and previous experience, for a certain beam, we can select the CIR value under a 100% coverage requirement (i.e., the CIR for the edge user, which is the worst), or under an 85% coverage requirement or under other coverage requirements. This method can take both the actual situation and engineering experience into account and is highly practical. However, it requires the real pattern of each antenna as the input, which is not convenient for theoretical research and model demonstration.
- (3) **Calculate values statistically:** The Monte Carlo simulation method is applied to randomly generate the locations of the target user and interfering users. In addition, we assume that there is only one user working in each interference area. The CIR in this specific scenario can be calculated by the quantification method proposed before. Then, this procedure is repeated over and over again. Finally, the probability density function (PDF) or cumulative distribution function (CDF) of the CIR can be obtained by statistics, and the value range of CIR can also be known. Generally, the CIR with the largest occurrence probability is selected. The detail process is shown in Figure 9.

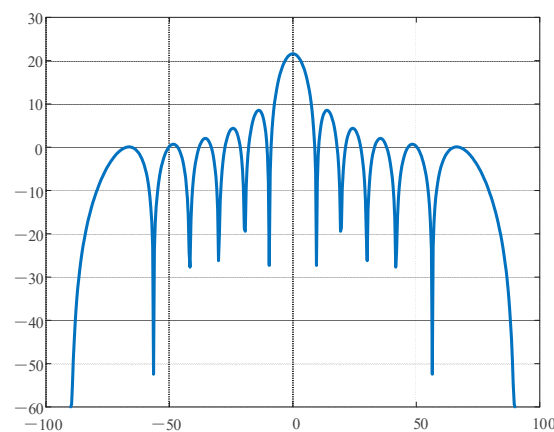


Figure 8. Example of the antenna radiation pattern.

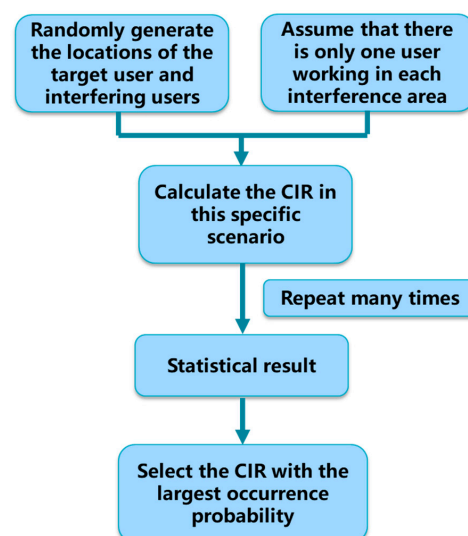


Figure 9. The detailed process of the Monte Carlo simulation method.

5. Analysis of the CIR under Different Frequency Plans

The adjustment of the frequency plan will directly affect the degree of interference between the co-channel beams. The variation in the interference degree will cause the variation in the CIR (and hence the carrier to interference and noise ratio, CINR), which will affect the system's capacity.

This section takes 19 beams with 4-color reuse (single polarization) as an example. Assuming two different beam-to-color mapping schemes, namely, regular mapping and irregular mapping, are adopted, we analyze the user-link CIR of each beam under them, respectively, by using the quantization method described in Section 3 and the statistical method described in Section 4. Furthermore, it can provide an idea for our future exploration, namely, frequency planning optimization based on CIR optimization.

The two mapping schemes, regular mapping and irregular mapping, are shown in Figure 10a,b, respectively. For regular mapping, the cell-center points of beams with the same color (except beam 1) always form a rectangular shape. Meanwhile, for irregular mapping, these points may form a parallelogram or a hexagon, not like in regular mapping with a rectangular shape. In addition, an important difference between these two mapping schemes is that the minimum spacing between beams with the same color for regular mapping is smaller than that for the irregular one. Each color corresponds to a certain frequency band, that is, the beams with the same color shall share the same uplink/downlink frequency band, and the interferences will appear among them consequently. In this simulation, we assume a Ka-band HTS for illustrative purposes and the simulation conclusion is also applicable to the satellite systems using other frequency bands, such as Ku. Specifically, the red color represents the uplink frequency of 27,500–28,125 MHz and the downlink frequency of 17,700–18,325 MHz, as shown on beams 4/7/9/11/15/17 in Figure 10a and beams 1/9/11/13/15/17/19 in Figure 10b. The yellow color represents the uplink frequency of 28125–28750 MHz and the downlink frequency of 18,325–18,950 MHz, as shown on beams 2/6/12/14 in Figure 10a and beams 2/5/12/18 in Figure 10b, respectively. The green color represents the uplink frequency of 28,750–29,375 MHz and the downlink frequency of 18,950–19,575 MHz, as shown on beams 3/5/8/18 in Figure 10a and beams 3/6/8/14 in Figure 10b, respectively. The orange color represents the uplink frequency of 29,375–30,000 MHz and the downlink frequency of 19,575–20,200 MHz, as shown on beams 1/10/13/16/19 in Figure 10a and beams 4/7/10/16 in Figure 10b, respectively. It is worth noting that these frequency values are taken only as an example and can be replaced by other values according to the actual situation.

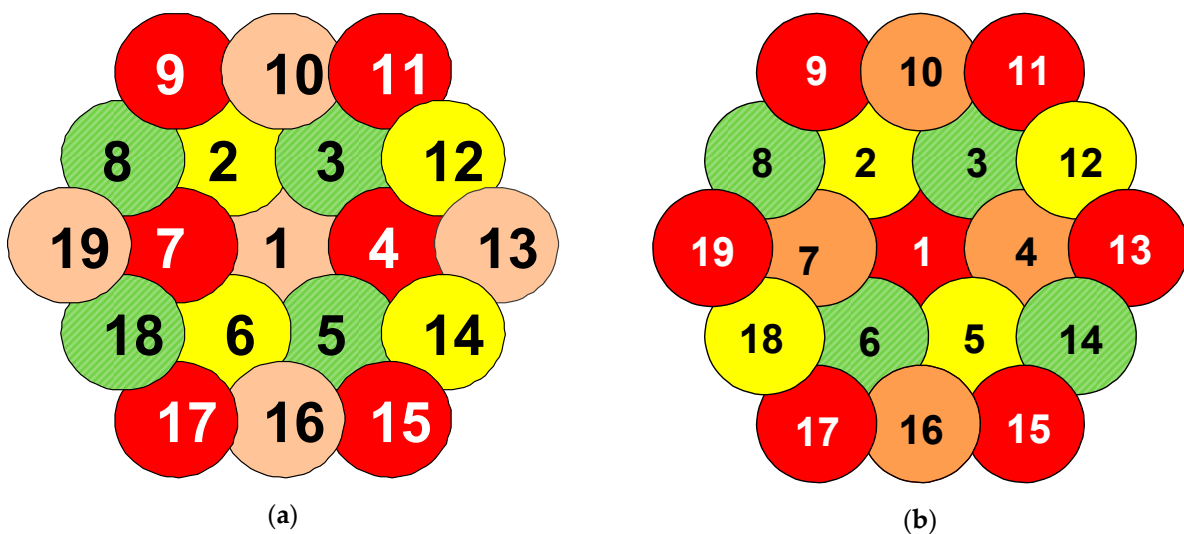


Figure 10. Two mapping schemes of 19 beams with 4 colors: (a) regular mapping and (b) irregular mapping.

The -3 dB beamwidths of the 19 beams are all assumed to be 0.25° . UPC is considered for the uplink of each beam, and the output power of the downlink travelling wave tube (TWT) is 100 W. Moreover, the sub-satellite point (i.e., the intersection points of the line segment, from the satellite to the Earth’s core, and the Earth’s surface) is in beam 1. The gain function of the onboard user antenna is as follows [13]:

$$g(\delta) = 51.5 - 12 \times (\delta/\theta_{-3\text{dB}})^2. \tag{24}$$

where δ refers to the deviation angle between the user link and antenna center, $0 < \delta \leq 2\theta_{-3\text{dB}}$, and δ is specified in degrees. $g(\delta)$, specified in dBi, is the antenna gain value when the deviation angle is δ . Finally, 51.5 is the peak gain in dBi, and $\theta_{-3\text{dB}}$ is the -3 dB width of the beam in degree.

In the simulation, the locations of the target user and interfering users in their respective areas are randomly generated and repeated 1000 times to obtain the cumulative distribution function of user-link CIR in 19 beams under different schemes. Taking beam 1 as an example (the other beams are similar), we compare and illustrate the influence of the two schemes on the cumulative distribution function of the CIR, as shown in Figure 11.

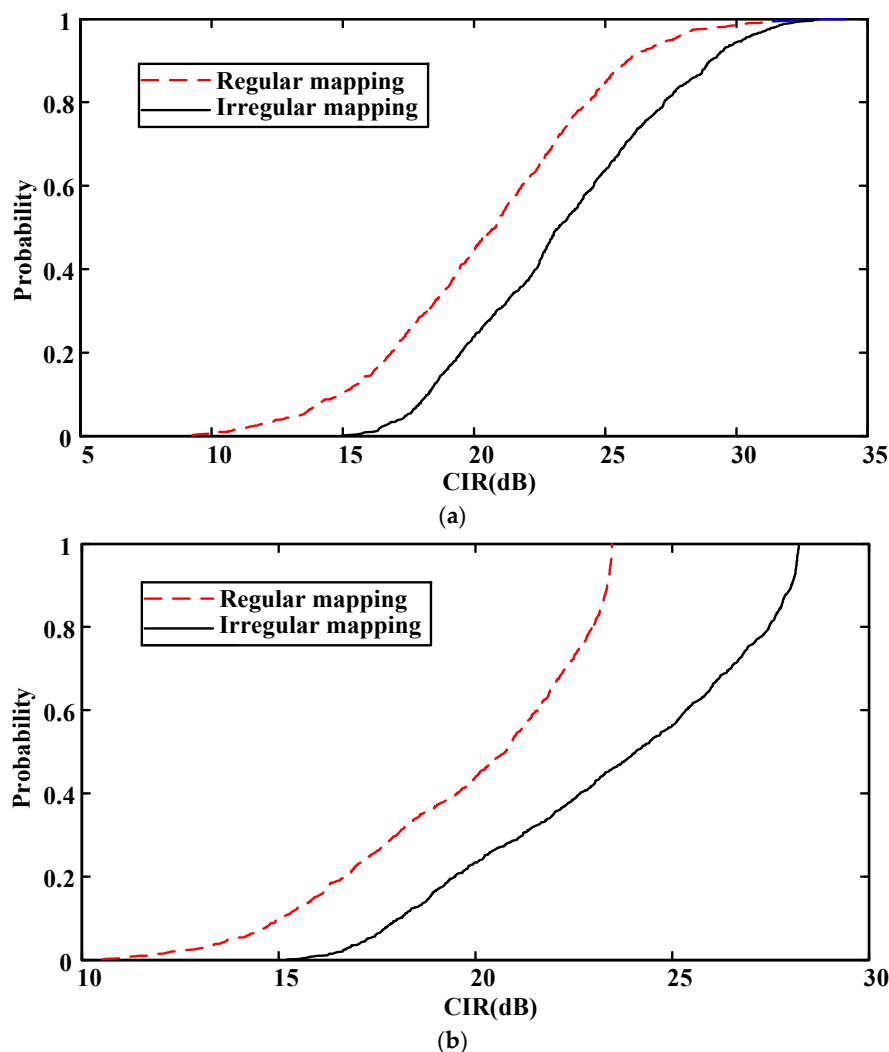


Figure 11. CDF of the CIR in the user link of beam 1 for the two mapping schemes: (a) user uplink and (b) user downlink.

A point on any line in Figure 11 has the following meaning. If the point coordinate is (x, y) , it means that the number of CIR results lower than x in this 1000-times simulation

is $1000 \times y$. For two comparative lines, if point A is on line 1, point B is on line 2, the horizontal coordinates of A and B are both equal to x , and the horizontal coordinates of A and B are y_1 and y_2 and $y_1 < y_2$, respectively, we can easily derive that the number of CIR results lower than x in this 1000-times simulation is $1000 \times y_1$ for line 1, while this value is $1000 \times y_2$ for line 2. It is evident that line 1 corresponds to a better scheme in terms of the CIR level. Hence, we can conclude that the lower line is better for the result shown in Figure 11.

It can be seen from Figure 11 that in 1000 simulation cases, for the user uplink of beam 1, the minimum CIR value under regular mapping is lower than 10 dB, while the minimum CIR value under irregular mapping is higher than 15 dB. Moreover, the corresponding maximum CIR values under the two schemes are similar. For the user downlink of beam 1, the minimum and maximum CIR values under regular mapping are lower than 11 dB and 24 dB, respectively, while the corresponding values under irregular mapping are higher than 15 dB and 28 dB. Specifically, with 20 dB as the reference value, the probability of meeting the reference value under regular mapping and irregular mapping is about 60% and 80%, respectively, regardless of the user uplink or downlink in beam 1. Therefore, irregular mapping is significantly better than regular mapping in terms of beam 1. In order to comprehensively consider all 19 beams, the CIR values satisfying the requirements of 100% coverage and 85% coverage are taken as the reference to compare the two schemes for all beams. The CIR of the user uplink and downlink are shown in Tables 1 and 2, respectively. In order to show the comparison effect more clearly, bar charts comparing the CIR of the user uplink and downlink for all beams with the 85% coverage requirement (the other coverage requirements are similar) are formed, as shown in Figure 12a,b, respectively.

Table 1. Comparison table of the carrier-to-interference ratio in the user uplink for all beams.

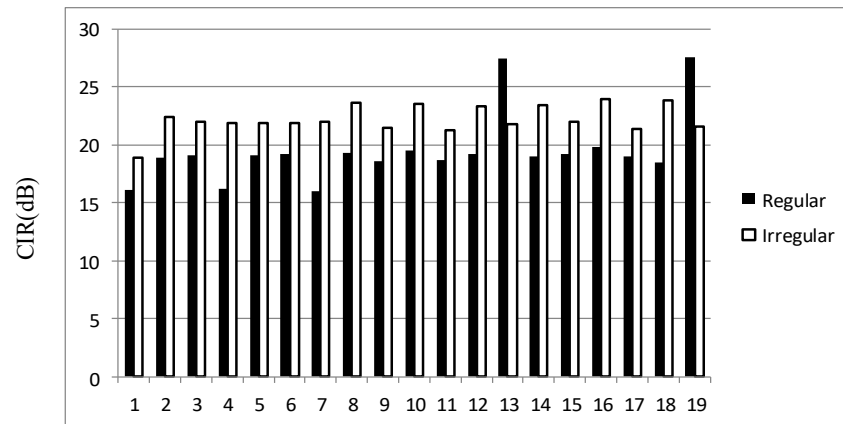
Beam Number	Regular Mapping (100%)	Irregular Mapping (100%)	Regular Mapping (85%)	Irregular Mapping (85%)
1	9.2606	14.9872	16.1319	18.8604
2	10.1616	15.7991	18.9329	22.4388
3	9.7408	16.7809	19.0899	21.9736
4	9.2041	15.6368	16.2649	21.9257
5	10.6164	15.7865	19.0899	21.8716
6	11.0048	15.9146	19.2189	21.9125
7	9.4866	15.9254	15.9918	22.0282
8	10.5623	16.9951	19.3401	23.6119
9	9.7729	16.5677	18.5994	21.4943
10	10.6398	17.7289	19.5461	23.5022
11	9.2702	15.4436	18.68	21.2889
12	9.6569	16.4399	19.1841	23.321
13	18.0649	15.9106	27.4372	21.789
14	9.3171	16.9615	19.0155	23.4624
15	10.1923	15.5998	19.2336	22.0265
16	10.5565	16.649	19.817	23.9043
17	9.861	14.891	19.0231	21.3366
18	9.9357	17.218	18.515	23.8914
19	18.0131	16.425	27.5559	21.6098

Table 2. Comparison table of the carrier-to-interference ratio in the user downlink for all beams.

Beam Number	Regular Mapping (100%)	Irregular Mapping (100%)	Regular Mapping (85%)	Irregular Mapping (85%)
1	10.5296	15.2191	15.9492	18.8482
2	11.0308	15.5642	19.1742	21.7539
3	10.599	15.4638	18.8925	21.6094
4	9.2715	15.9482	16.3099	21.9943

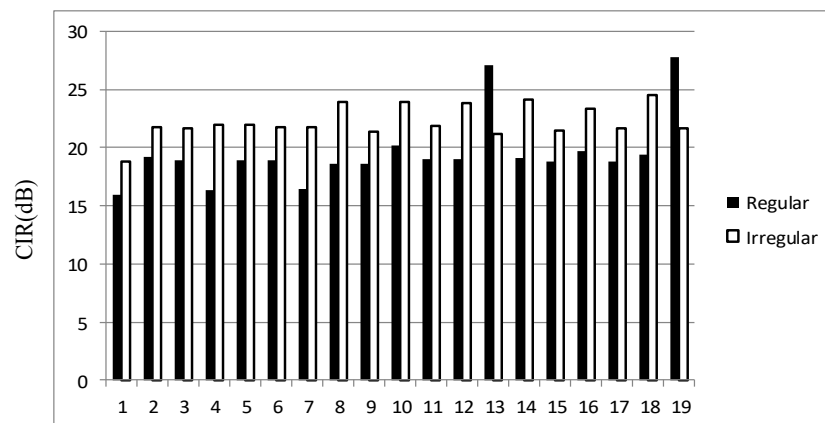
Table 2. Cont.

Beam Number	Regular Mapping (100%)	Irregular Mapping (100%)	Regular Mapping (85%)	Irregular Mapping (85%)
5	9.7372	15.67	18.8735	21.9992
6	10.2384	15.1158	18.8889	21.764
7	9.8431	15.1892	16.4151	21.7531
8	9.9244	15.8582	18.6233	23.971
9	10.2184	15.9944	18.5536	21.3466
10	9.5335	15.5228	20.1408	23.932
11	10.0657	15.6549	18.9683	21.8409
12	9.349	16.0712	18.9951	23.8069
13	18.0882	15.6842	27.0678	21.1188
14	9.7735	16.5255	19.0928	24.0822
15	9.2774	15.2369	18.7801	21.4129
16	10.1376	16.1157	19.729	23.2872
17	11.1235	15.4051	18.7778	21.6125
18	10.5613	15.6464	19.368	24.5192
19	17.977	15.5814	27.7218	21.7026



Beam number

(a)



Beam number

(b)

Figure 12. Comparison diagram of the CIR in all beams for 85% coverage: (a) user uplink and (b) user downlink.

It can be seen from Table 1 and Figure 12 that the CIR values of the user uplink and downlink obtained by irregular mapping are higher than those obtained by regular mapping in all of the beams, except for beam 13 and beam 19 whose values are highlighted

in bold. In addition, irregular mapping can make the CIR of the user uplink or downlink more balanced for all of the beams. Specifically, as shown in Figure 6, the variance in the user-uplink CIR in all beams obtained by regular mapping is 8.735, and the variance is 8.542 for user downlink. However, the variance in the user uplink CIR and user downlink CIR is only 1.393 and 1.805 under irregular mapping, respectively.

From the above simulation cases, it is obvious that the frequency plan has a significant impact on the CIR. In general, the larger the minimum spacing between the beams at the same frequency (maximizing the minimum spacing at the same frequency), the better the system's CIR performance. Therefore, we can follow the above idea to explore the optimization scheme of the frequency plan based on the improvement of the CIR.

6. Analysis of the CIR under Different Power Spectral Density (PSD)

In this section, we conduct a simulation analysis of the CIR under different PSD. The number of beams, the beam layout, the -3 dB beamwidth of all the beams, and the gain function of the onboard user antenna are the same as those in Section 4. In addition, the frequency plan adopts 4-color regular mapping, as shown in Figure 10a. What is particular about this simulation setup is that the output power of downlink TWTs for all the beams are different. In detail, in order to cover more potential cases concerning how different PSD levels are distributed among the co-channel beams, the output power of downlink TWTs are set to 80 W, 100 W, 80 W, 60 W, 80 W, 100 W, 80 W, 80 W, 100 W, 100 W, 80 W, 100 W, 100 W, 100 W, 100 W, 80 W, 80 W, and 100 W for beams 1~19, respectively. The PSD is obtained as a mean value for each TWT/transponder, i.e., power/bandwidth. It can be concluded that the PSD levels of all the beams are not the same due to their equal bandwidth and unequal transmit power.

The locations of the target user and interfering users in their respective areas are randomly generated and repeated 1000 times to obtain the cumulative distribution function of the user link CIR in 19 beams. Taking beam 1 as an example (the other beams are similar), we illustrate the cumulative distribution function of the CIR in Figure 13, represented by a solid line. In order to present the comparative effect concerning different or uniform PSD, we also put the previous simulation result in Figure 13, as shown as the dotted line, which is achieved in Section 4 when assuming all of the downlink TWTs as 100 W.

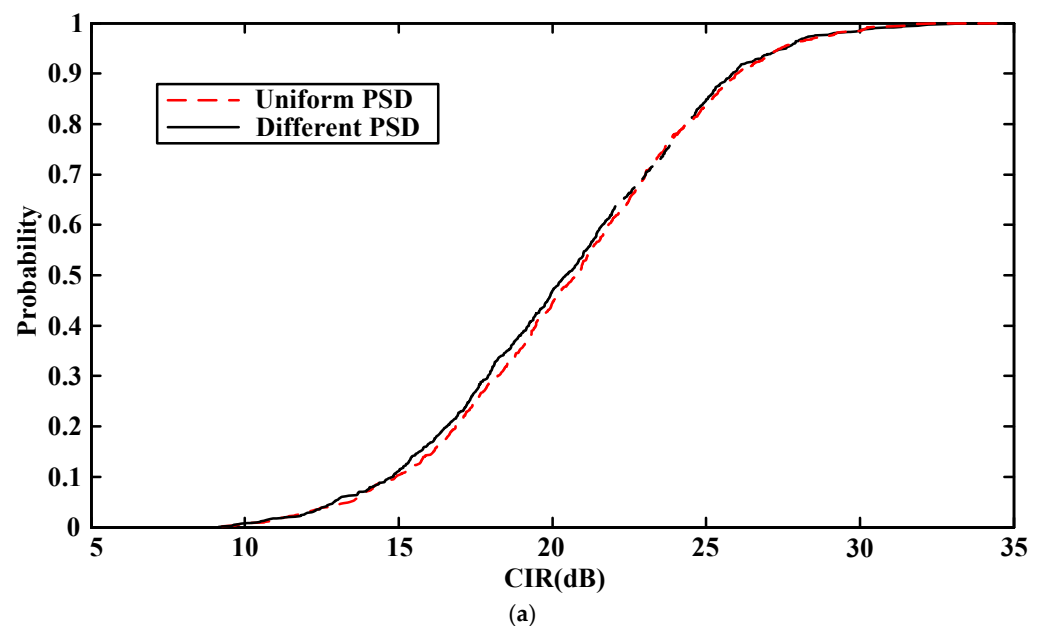


Figure 13. Cont.

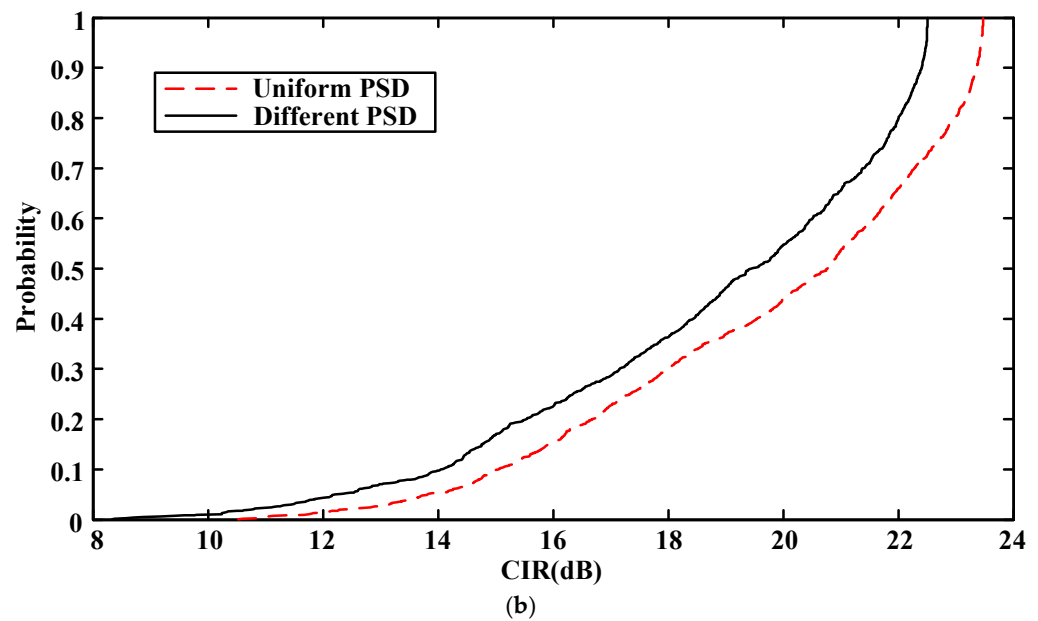


Figure 13. CDF of the CIR in the user link of beam 1 concerning different or uniform PSD: (a) user uplink and (b) user downlink.

It can be seen from Figure 13a that the CIR levels are almost the same for the user uplink of beam 1, regardless of different or uniform PSD. The reason for this is that we set the different PSD by adjusting the output power of the downlink TWTs, while keeping the output power of user terminals unchanged. In other words, only the downlink's PSD is varied. As shown in Figure 13b, for the user downlink of beam 1, the CIR level under different PSD is evidently lower than that under uniform PSD. The reason is as follows. The user downlink PSD of beam 1, $80 \text{ W}/(20,200\text{--}19,575) \text{ MHz}$, suffers from a significant decrease compared to that under uniform PSD, $100 \text{ W}/(20,200\text{--}19,575) \text{ MHz}$. Meanwhile, the user downlink PSD of beam 10/13/16/19, which shares the same frequency band as beam 1, remains unchanged. In other words, the carrier signal power of beam 1 decreases while the interference power remains constant.

In order to comprehensively conduct an analysis of all 19 beams, the CIR values satisfying the requirements of 100% coverage and 85% coverage are taken as the reference. Moreover, the CIR levels are almost the same for the user uplink regardless of different or uniform PSD, which is inferred from beam 1 to all the beams. Therefore, not paying useless attention to the user uplink, we only simulate the user downlink CIR of all the beams under both different and uniform PSD, as shown in Table 3. In order to show the comparison effect under different and uniform PSD more clearly, bar charts illustrating the user downlink CIR of all beams with the 85% coverage requirement (the other coverage requirements are similar) are formed, as shown in Figure 14.

It can be seen from Table 3 and Figure 14 that the size relation of user downlink CIR values under different PSD and uniform PSD is uncertain among the 19 beams. In particular, for co-channel beam group 1 (beams 1, 10, 13, 16, and 19), the user downlink CIR level of beam 1 under different PSD is lower than that under uniform PSD, which has been explained before; the user downlink CIR level of beams 10/13/16/19 under different PSD is higher than that under uniform PSD because their downlink PSD levels remain unchanged while the interference power coming from beam 1 decreases evidently. For co-channel beam group 2 (beams 2, 6, 12, and 14), the simulation results change very weakly under different PSD compared to uniform PSD, due to the unchanged PSD of beams 2/6/12/14. For co-channel beam group 3 (beams 3, 5, 8, and 18), the simulation results also change weakly because the carrier signal power and interference power decrease at almost the same level for any beam therein. For co-channel beam group 4 (beams 4, 7, 9, 11, 15, and 17), the situations are diverse. The user downlink CIR level of beam 4 decreases

significantly under different PSD compared to uniform PSD because beam 4 suffers from a significantly downward carrier signal power while it benefits from downward interference power slightly. The user downlink CIR level of beams 9/15 experiences an increase under different PSD compared to uniform PSD due to the unchanged carrier signal power and downward interference power. The user downlink CIR level of beams 7/11/17 shows an uncertain and slight change under different PSD compared to uniform PSD. It depends on which one of the carrier signal power and interference power decreases more, although neither of them decreases significantly.

Table 3. Comparison table of the carrier-to-interference ratio in the user downlink for all beams.

Beam Number	Uniform PSD (100%)	Different PSD (100%)	Uniform PSD (85%)	Different PSD (85%)
1	9.1476	8.3283	15.4757	15.2858
2	10.2235	9.6809	18.6396	18.6238
3	9.7086	9.6059	18.7088	18.5805
4	9.3834	7.8223	15.9323	14.7389
5	9.4736	9.7096	18.4205	18.7714
6	9.682	10.2256	18.8294	18.8342
7	8.1256	8.4698	16.2136	16.0486
8	9.6299	9.793	18.7278	18.2061
9	9.4446	10.6242	18.9664	19.9392
10	10.1862	10.7314	20.2076	20.7228
11	9.3382	11.0702	18.8319	19.0194
12	9.7437	9.1889	18.6784	18.5162
13	18.0204	18.9792	27.8481	28.0972
14	9.1908	9.7679	18.8117	18.5068
15	9.8039	12.334	18.4607	20.8107
16	9.3163	10.4101	19.5754	20.4748
17	9.1078	9.7934	18.9443	18.5562
18	9.8011	9.6168	18.5621	18.6951
19	18.2461	18.9855	27.8347	29.2076

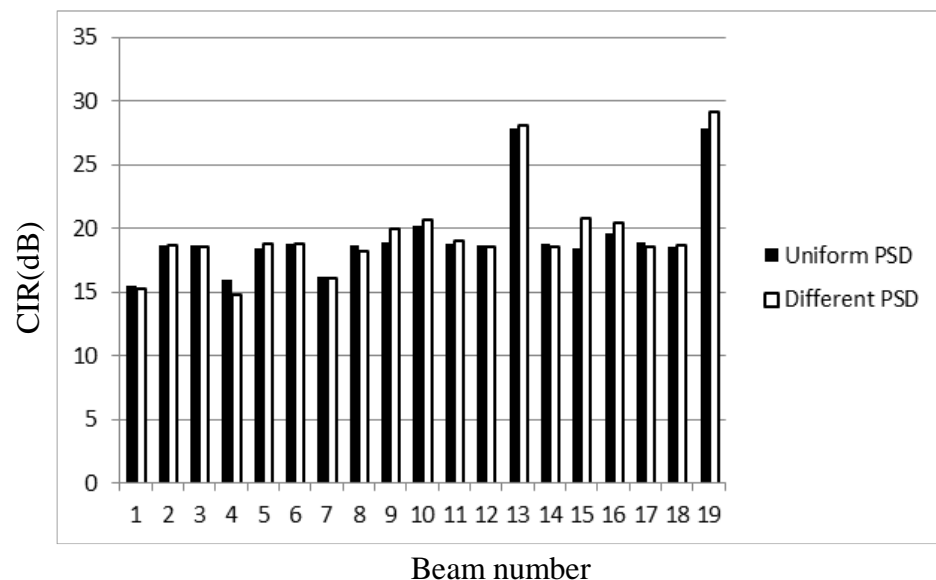


Figure 14. Comparison diagram of the user downlink CIR in all beams for 85% coverage.

Furthermore, we can conclude the importance of the estimation of the CIR with PSD, which accords with our method very well, for satellite operators, especially in the present day’s flexible payload applications. Flexible payload architectures can support configurable power, bandwidth, and/or coverage, which provides operators with flexibilities but also challenges. For example, in order to change the in-orbit capacity of one beam according

to real-time demand, the operator can reallocate the channel power among several beams. However, it will affect the PSD of beams, and then yield variation in the beam's CIR, which can even lead to link interruption. Therefore, the operators will be overcautious during the power allocation. Our work is so meaningful in that it provides operators with prediction of beams' CIR after power allocation and helps them to find a possible allocation scheme guaranteeing the level of beams' CIR.

7. Conclusions

In view of the booming trend of multi-beam HTS, the necessity of precise quantification and analysis of the CIR concerning the co-channel interference caused by frequency reuse is first discussed in this paper. Starting from the different mechanisms of uplink and downlink interference, the quantification methods of uplink and downlink interferences are discussed and the closed-form expressions are given. Furthermore, the influencing factors and selection strategies are summarized. The proposed quantification method and Monte Carlo selection strategy are verified through simulation.

For the system of 19 beams with 4-color reuse (single-polarization), it can be seen from the simulation results that different frequency plans have significant effects on the cumulative distribution function of the CIR of each beam and the variance in the CIR of all beams. The larger the minimum spacing between the beams at the same frequency (maximizing the minimum spacing at the same frequency), the better the system's CIR performance. Therefore, we can follow the idea to explore better frequency plans.

Moreover, based on the simulation analysis of the CIR under different PSD, the variation in user downlink CIR values with PSD is uncertain, and we give a detailed analysis of the causes. Furthermore, we derive the importance of our work in satellite operations. It can provide the operators with prediction of beams' CIR after power allocation and help them to find a possible allocation scheme, guaranteeing the level of beams' CIR.

Author Contributions: Conceptualization, Z.D. and P.Q.; formal analysis, Z.D. and L.Y.; funding acquisition, Y.Z. and C.Z.; investigation, Z.D. and P.Q.; methodology, Z.D. and L.Y.; software, Z.D. and C.Z.; validation, Y.Z. and C.Z.; writing—original draft, Z.D.; writing—review and editing, K.L. All authors have read and agreed to the published version of the manuscript.

Funding: This research was supported by the pre-research project on Civil Aerospace Technologies, grant number D010203.

Data Availability Statement: No new data were created or analyzed in this study. Data sharing is not applicable to this article.

Conflicts of Interest: The authors declare no conflict of interest. The funders had no role in the design of the study; in the collection, analysis, or interpretation of the data; in the writing of the manuscript; or in the decision to publish the results.

References

1. Zhao, Z.; Du, Q.; Wang, D. Overview of Prospects for Service-Aware Radio Access towards 6G Networks. *Electronics* **2022**, *11*, 1262. [[CrossRef](#)]
2. Camino, J.T.; Artigues, C.; Houssin, L. Mixed-Integer Linear Programming for Multibeam Satellite Systems Design: Application to the Beam Layout Optimization. In Proceedings of the 2016 Annual IEEE Systems Conference (SysCon), Orlando, FL, USA, 18–21 April 2016.
3. Tao, C.; Zhang, L.; Wang, Y. An Extended Configuration Design of High-Throughput Satellite. *J. Phys. Conf. Ser.* **2022**, *2396*, 012049. [[CrossRef](#)]
4. Lutz, E.; Werner, M.; Jahn, A. *Satellite Systems for Personal and Broadband Communications*; Springer: Berlin/Heidelberg, Germany, 2000.
5. Lutz, E. Achieving a terabit/s GEO satellite system. In Proceedings of the 19th Ka and Broadband Communications, Florence, Italy, 14–17 October 2013.
6. Guan, Y.; Geng, F.; Saleh, J.H. Review of High Throughput Satellites: Market Disruptions, Affordability-Throughput Map, and the Cost Per Bit/Second Decision Tree. *IEEE Aerosp. Electron. Syst. Mag.* **2019**, *34*, 64–80. [[CrossRef](#)]
7. Perez-Neira, A.I.; Vazquez, M.A.; Shankar, M.R.B. Signal Processing for High Throughput Satellite Systems: Challenges in New Interference-Limited Scenarios. *IEEE Signal Process. Mag.* **2019**, *36*, 112–131. [[CrossRef](#)]

8. Widjanarko, D.; Gunawan, D. A Hybrid C/Ku-band High Throughput Satellite Systems as An Optimal Design for Indonesia. In Proceedings of the 2017 International Conference on Signals and Systems (ICSigSys), Bali, Indonesia, 16–18 May 2017.
9. Caus, M.; Perez-Neira, A.I.; Angelone, M. An innovative interference mitigation approach for high throughput satellite systems. In Proceedings of the IEEE 16th International Workshop on Signal Processing Advances in Wireless Communications (SPAWC), Stockholm, Switzerland, 27 June–1 July 2015.
10. Evans, B.; Thompson, P. Key issues and technologies for a Terabit/s satellite. In Proceedings of the 28th AIAA International Communications Satellite Systems Conference (ICSSC-2010), Anaheim, CA, USA, 30 August–2 September 2010.
11. Serrano-Velarde, D.; Lance, E.; Fenech, H. Novel Dimensioning Method for High-Throughput Satellites: Forward Link. *IEEE Trans. Aerosp. Electron. Syst.* **2014**, *50*, 2146–2163. [[CrossRef](#)]
12. Ortiz-Gomez, F.G.; Salas-Natera, M.A.; Martínez, R.; Landeros-Ayala, S. Optimization in VHTS Satellite System Design with Irregular Beam Coverage for Non-Uniform Traffic Distribution. *Remote Sens.* **2021**, *13*, 2642. [[CrossRef](#)]
13. Fenech, H. *High-Throughput Satellites*; Artech House: Boston, MA, USA, 2021.
14. Vasavada, Y.; Gopal, R.; Ravishankar, C. Architectures for next generation high throughput satellite systems. *Int. J. Satell. Commun. Netw.* **2016**, *34*, 523–546. [[CrossRef](#)]
15. Ortiz-Gomez, F.G.; Martínez, R.; Salas-Natera, M.A.; Cornejo, A.; Landeros-Ayala, S. Forward Link Optimization for the Design of VHTS Satellite Networks. *Electronics* **2020**, *9*, 473. [[CrossRef](#)]
16. Kyrgiazos, A.; Evans, B.; Thompson, P. A terabit/second satellite system for European broadband access: A feasibility study. *Int. J. Satell. Commun. Netw.* **2014**, *32*, 63–92. [[CrossRef](#)]
17. Al-Hraishawi, H.; Chougrani, H.; Kisseleff, S. A survey on non-geostationary satellite systems: The communication perspective. *IEEE Commun. Surv. Tutor.* **2022**, *25*, 101–132. [[CrossRef](#)]
18. Álvarez, G.; Fraire, J.A.; Hassan, K.A. Uplink transmission policies for LoRa-based direct-to-satellite IoT. *IEEE Access* **2022**, *10*, 72687–72701. [[CrossRef](#)]
19. Tondo, F.A.; Montejó-Sánchez, S.; Pellenz, M.E. Direct-to-satellite IoT slotted aloha systems with multiple satellites and unequal erasure probabilities. *Sensors* **2021**, *21*, 7099. [[CrossRef](#)] [[PubMed](#)]
20. Tondo, F.A.; Souto, V.D.P.; López, O.L.A. Optimal Traffic Load Allocation for Aloha-Based IoT LEO Constellations. *IEEE Sens. J.* **2022**, *23*, 3270–3282. [[CrossRef](#)]
21. Afhamisis, M.; Palattella, M.R. SALSA: A scheduling algorithm for LoRa to LEO satellites. *IEEE Access* **2022**, *10*, 11608–11615. [[CrossRef](#)]
22. Capez, G.M.; Henn, S.; Fraire, J.A.; Garello, R. Sparse satellite constellation design for global and regional direct-to-satellite IoT services. *IEEE Trans. Aerosp. Electron. Syst.* **2022**, *58*, 3786–3801. [[CrossRef](#)]
23. Wang, J.; Li, K.; Geng, Y.; He, Y. Satellite Communication Coding Design Based on Large Frequency Reuse Factor and Precoding Technology. In Proceedings of the 2023 IEEE International Conference on Control, Electronics and Computer Technology (ICCECT), Shenzhen, China, 19–21 June 2023.
24. Abass, E.S.; Halim, J.V.M.; Hennawy, H.E. Capacity Enhanced High Throughput Satellite-Coded-Beams resource management strategy. In Proceedings of the 2023 International Microwave and Antenna Symposium (IMAS), Cairo, Egypt, 7–9 February 2023.
25. Kodheli, O.; Maturo, N.; Shankar, B. Satellite Communications in the New Space Era: A Survey and Future Challenges. *IEEE Commun. Surv. Tutor.* **2021**, *23*, 70–109. [[CrossRef](#)]
26. Ramírez, T.; Mosquera, C.; Alagha, N. Flexible User Mapping for Radio Resource Assignment in Advanced Satellite Payloads. *IEEE Trans. Broadcast.* **2022**, *68*, 723–739. [[CrossRef](#)]

Disclaimer/Publisher’s Note: The statements, opinions and data contained in all publications are solely those of the individual author(s) and contributor(s) and not of MDPI and/or the editor(s). MDPI and/or the editor(s) disclaim responsibility for any injury to people or property resulting from any ideas, methods, instructions or products referred to in the content.